Langmuir

Article

pubs.acs.org/Langmuir

High-Performance Visible-Light-Driven Plasmonic Photocatalysts Ag/AgCl with Controlled Size and Shape Using Graphene Oxide as Capping Agent and Catalyst Promoter

Mingshan Zhu,[†] Penglei Chen,*[,†,‡] and Minghua Liu*[,†]

[†]Beijing National Laboratory for Molecular Science, CAS Key Laboratory of Colloid, Interface and Chemical Thermodynamics, Institute of Chemistry, Chinese Academy of Sciences, No. 2 Zhongguancun Beiyijie, Beijing 100190, People's Republic of China

[‡]College of Chemistry and Molecular Engineering, Zhengzhou University, 100 Science Road, Zhengzhou, Henan 450001, People's Republic of China

Supporting Information

ABSTRACT: We report herein that Ag/AgCl-based plasmonic photocatalysts with controlled size and shape could be easily formulated by a one-pot approach via a precipitation reaction between $AgNO_3$ or $Ag(NH_3)_2NO_3$ and NaCl. It is found that near-spherical and cube-like Ag/AgCl nanoarchitectures of 500 nm could be fabricated at lower and higher temperature, respectively. Fascinatingly, when graphene oxide (GO) nanosheets are introduced into the synthesis medium, the size of the formulated near-spherical and cube-like nanostructures, Ag/AgCl/GO, could be 2.5 and 5 times reduced to ca. 200 and 100 nm, respectively, when $AgNO_3$ and $Ag(NH_3)_2NO_3$ are employed as the silver source. The series of our Ag/AgCl-based nanostructures could be used as visible-light-driven plasmonic photocatalysts for the photodegradation of methyl orange pollutants, wherein the cube-like Ag/AgCl/GO nanoarchitectures of 100 nm display the highest catalytic activity. It is disclosed that the synergistic effect of size, shape, and GO nanosheets plays an important role for their boosted photocatalytic performances. The investigation reveals that GO nanosheets work not only as a capping agent for a controllable fabrication of Ag/AgCl nanostructures, but also as catalyst promoter during the photocatalytic performances, leading to an enhanced catalytic activity. Our unique GO-assisted method likely paves a facile avenue and initiates new opportunities for the exploration of GO-hybridized high-performance catalysts.

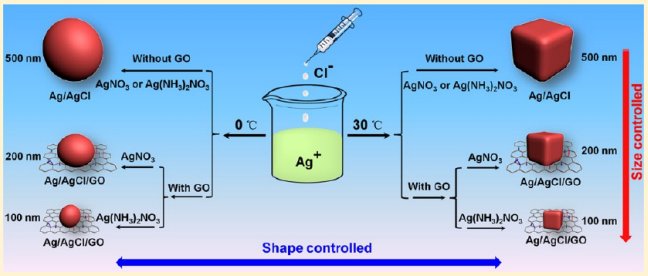

INTRODUCTION

During the last decades, nanostructured materials with controlled size and shape have gained broad interests in scientific and technological communities.[1−7] This is due to their size- and shape-selective physicochemical properties, which enable them to be promising candidates in a variety of fields of paramount importance,[1−7] especially in the area of catalysis.[4−7] This is mainly embodied in their unique size- and shape-dependent catalytic performances, which pave attractive avenues for the construction of highly efficient catalysts.[4−7] The size-sensitive catalytic performances could be understood in light of the distinct surface-to-volume ratio of nanospecies of different sizes, which could arouse variations in the amount of the catalytically active sites per mass, and the electronic and geometric properties that dominate the activation and adsorption/desorption of the involved reactants. The shape-selective catalytic activity could be interpreted in terms of the different reaction performances induced by the specific crystal facets selectively exposed by an anisotropically shaped nanostructure, and also the amount of the catalytically active sites, such as corners, edges, steps, etc.[4−7] Accordingly, it is an issue of considerable concern to synthetically achieve a controllable fabrication of nanomaterials with tuned size and shape. This might initiate new forums for the achievement and identification of high-performance catalysts.

In the frontier area of catalysis, it is currently a hot topic that plasmonic photocatalysts featured with distinct surface plasmon resonance (SPR) absorptions over a wide range of visible-light region are promising materials as high-performance visible-light-energized photocatalysts.[8−27] Among diverse plasmonic photocatalytic systems, Ag/AgCl-based species have received particular attention, due to their outstanding visible-light-responsive photocatalytic performances, although AgCl is traditionally used as the primary source material in photosensitive plates and is unstable upon photoirradiation.[11,15−17,20−27] Several efforts have been devoted to the synthesis of shaped Ag/AgCl nanomaterials,[17,22−27] wherein template-mediated protocols are frequently used.[17,23−27] However, the challenge of synthetically controlling the size and shape of the produced Ag/AgCl nanospecies has been met

Received: April 18, 2013
Revised: July 1, 2013
Published: July 2, 2013

Scheme 1. A Schematic Illustration for the Fabrication of Ag/AgCl-Based Nanostructures with Controlled Size and Shape[a]

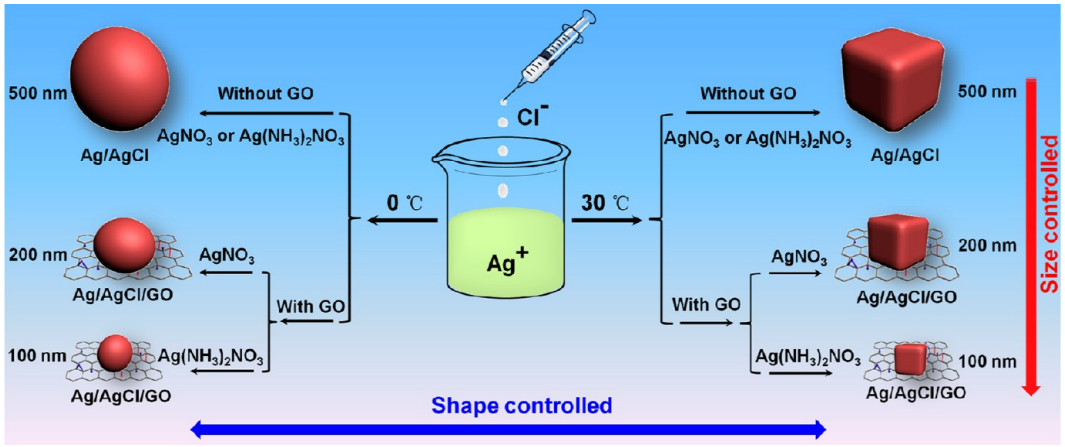

[a]The drawings are not to scale.

with limited success, although an investigation on this issue might provide an important platform for the exploration of their size- and shape-sensitive photocatalytic performances, and thus favors an optimized selection of high-quality plasmonic photocatalysts. Moreover, the employed templates, generally amphiphilic surfactants, ionic liquids, or polymers, could only play an important role during the synthesis step. After the nanofabrication, tremendous efforts have to be carried out to remove the templates, because these templates themselves could not work as catalyst promoter in the subsequent photocatalytic step. Considering the broad interest of plasmonic photocatalyst[8−19] and the general significance of size- and shape-dependent catalytic properties as well,[4−7] a synthetically controllable fabrication of Ag/AgCl nanostructures with controlled size and shape using a functional template, the template employed during the nanofabrication step could work as a catalyst promoter in the catalytic step, is an important subject that remains to be explored.

Currently, graphene oxide (GO), a novel graphene derivative whose basal plane and edge are decorated with diverse oxygen-containing functional groups, including carboxyl, hydroxyl, epoxide, etc., has been verified to be an excellent catalyst carrier and promoter.[15,28−33] This is due to its astonishing large specific surface area, high optical transmittance, and unique electronic properties caused by the locally conjugated aromatic system.[15,31−33] Because of their appealing atomic thick two-dimensional structural character, and their intrinsic amphiphilic property that comes from the existence of hydrophilic oxygen-containing groups and the locally distributed hydrophobic π system, GO could be structurally regarded as unconventional polymers in a colloid system.[34−36] In virtue of these basic understandings, great expectations might be desired by introducing GO into the fabrication of the Ag/AgCl nanospecies with controlled size and shape, wherein GO works not only as the template in the synthesis step, but also as catalytic promoter in the photocatalytic step.

As a part of our sustained efforts in this topic,[15,19,20,22,23] we herein demonstrate that simply by a precipitation reaction between Cl^- of NaCl and Ag^+ of different silver sources ($AgNO_3$ and $Ag(NH_3)_2NO_3$, designated as $AgNO_3$ and $Ag(NH_3)_2NO_3$ systems, respectively, hereafter), near-spherical and cube-like Ag/AgCl of ca. 500 nm could be produced by controlling the temperature of the synthesis system (Scheme 1). Introduction of GO nanosheets into the synthesis system leads to the formation of Ag/AgCl/GO nanostructures, and, more interestingly, the size of these GO-hybridized nanostructures of different shape could be reduced by 2.5 times to ca. 200 nm in the case of $AgNO_3$ system, while it could further be reduced by 5 times to ca. 100 nm in the case of the $Ag(NH_3)_2NO_3$ system. The realization of synthetically controllable fabrication of Ag/AgCl nanospecies with controlled size and shape permits an optimized selection of high-performance plamonic photocatalysts. Among the series of the Ag/AgCl-based plasmonic photocatalysts of distinct size and shape, the cube-like GO-hybridized Ag/AgCl (Ag/AgCl/GO) of ca. 100 nm has been proved to be the most efficient catalytic species for the photodegradation of methyl orange (MO) pollutant under visible-light irradiation. The results show that its catalytic activity displays a significant enhancement by a factor of 20 as compared to the near-spherical bare Ag/AgCl of 500 nm. It is disclosed that the synergistic effect of size, shape, and GO nanosheets plays an important role for its substantially boosted catalytic activity. In our unique protocol, it is found that GO serves not only as a capping agent for a controllable nanofabrication of Ag/AgCl nanoarchitecture, but also as a catalyst promoter for the enhancement of their catalytic activities. Regarding the broad interests of GO and the significant concerns of visible-light-driven plasmonic photodegradation catalysts, our GO-mediated protocol might pave an easy avenue and open new opportunities for the investigation of GO-hybridized high-performance catalysts.

EXPERIMENTAL SECTION

Chemicals and Materials. Silver nitrate ($AgNO_3$, Sigma-Aldrich, >99%), ammonia solution ($NH_3{\cdot}H_2O$, 25−28%, Beijing Chemical Works), sodium chloride (NaCl, >99.5%, Beijing Chemical Works, A.R.), graphite powder (Alfa Aesar, 325mesh, 99.9995%), and methyl orange (MO, Alfa Aesar, >98%) were used as received without additional purification or treatment. Milli-Q water was used as the solvent for all of the solutions or dispersions.

Synthesis of Graphene Oxide (GO) Nanosheets. GO nanosheets were synthesized through a chemical exfoliation of graphite powder by using a modified Hummers' method. The detailed synthesis procedure was carried out according to the methods described previously.[15] As shown in Figure S1, the produced GO nanosheets were characterized by AFM and XRD investigations. The results show that our GO nanosheets have a lateral size of ca. 300−1000 nm and a thickness of ca. 0.85 nm. A diffraction peak around 10.48°, which

dx.doi.org/10.1021/la401473t | Langmuir 2013, 29, 9259−9268

indicates an interlayer distance of ca. 0.84 nm, is observed from their XRD pattern.

Controllable Synthesis of Ag/AgCl-Based Nanostructures. As shown in Scheme 1, Ag/AgCl and Ag/AgCl/GO with controlled size and shape could be formulated via a precipitation reaction between $AgNO_3$ or $Ag(NH_3)_2NO_3$ and NaCl. Specifically, for the synthesis of the GO-hybridized Ag/AgCl, Ag/AgCl/GO, wherein $AgNO_3$ was used as Ag source, a GO dispersion (500 μL, 1 mg mL^{-1}) was added dropwise to a 10 mL $AgNO_3$ solution (0.01 M) within 5 min under vigorous magnetic stirring. The temperature of the synthesis system was monitored at 0 or 30 °C by a water bath. Subsequently, a 500 μL NaCl solution (0.2 M) was dropwise injected into the above dispersion within ca. 5 min. After the addition of NaCl, the stirring was continuously maintained for another 20 min. The dispersion was treated by centrifugation (10 000 rpm, 10 min), and the produced solids were collected and washed thoroughly with ultrapure Milli-Q water by repeating centrifugations. Similar operations were carried out when $Ag(NH_3)_2NO_3$ was used as the Ag source, except that a 200 μL ammonia solution (1 M) was added dropwise to the $AgNO_3$ solution 5 min prior to the addition of GO and NaCl. This performance was intended to obtain $Ag(NH_3)_2NO_3$ solution. For bare Ag/AgCl, similar procedures were performed, except that no GO was involved during the synthesis.

Photocatalytic Performance. For catalytic experiments, 11 mg of Ag/AgCl-based nanospecies were dispersed in a 12 mL methyl orange (MO, 40 mg L^{-1}) solution, wherein a quartz cuvette was used as the reactor. A 500 W xenon arc lamp installed in a laboratory lamp housing system (CHF-XM35-500 W, Beijing Trusttech Co. Ltd., China) was employed as the light source. The light passed through a 10 cm water filter and a UV cutoff filter (>400 nm) before entering the reactor. The reaction system was kept for 30 min in a dark room to achieve an equilibrium adsorption state before visible-light irradiation. Aliquot of the dispersion (0.3 mL) was taken out from the reaction system for real-time sampling. The photodegradation of MO over our catalysts was investigated by measuring the real-time UV−vis absorption of MO at 463 nm. For the evaluation of the photocatalytic activities, C is the concentration of MO at a real-time t, and C_0 is the concentration in the MO solution immediately before it was kept in dark.

Fabrication of Electrodes and Electrochemical Impedance Spectral Measurements. For the electrochemical impedance spectral (EIS) measurement, the electrode was fabricated by a modification of glassy carbon (GC) electrode using our Ag/AgCl, GO, or Ag/AgCl/GO. Before modification, the GC electrode surface is polished with 0.3 μm alumina slurry, and then rinsed with water in an ultrasonic bath. Subsequently, ca. 1 mg of Ag/AgCl, GO, or Ag/AgCl/GO was dispersed in Nafion water solution under ultrasonic stirring, and the obtained paste was spread on the surface of GC electrode and dried under ambient condition.

The electrochemical impedance measurements were carried out on a conventional three-electrode cell using a CHI 660B potentiostat/galvanostat (Shanghai Chenhua Instrumental Co., Ltd., China) at room temperature, wherein the modified GC electrode served as the working electrode, with a platinum wire as the counter electrode and a saturated calomel (saturated KCl) electrode (SCE) as the reference electrode. The measurement was performed in the presence of a 2.5 mM $K_3[Fe(CN)_6]/K_4[Fe(CN)_6]$ (1:1) mixture as a redox probe in 0.1 M KCl solution. The impedance spectra were recorded with the help of ZPlot/ZView software under an ac perturbation signal of 5 mV over the frequency range from 10 kHz to 0.1 Hz at a potential of 0.1 V.

Apparatus and Measurements. The scanning electron microscopy (SEM) measurements were carried out by using a Hitachi S-4800 system. The AFM images without any processing except flattening were recorded on a Digital Instrument Nanoscope IIIa Multimode system (Santa Barbara, CA) with a silicon cantilever by using tapping mode. The energy dispersive X-ray spectroscopy (EDX) was measured with a Horiba EMAX X-act energy dispersive spectrometer that was attached to the Hitachi S-4800 system. X-ray diffraction (XRD) measurements were performed on a PANalytical X'Pert PRO instrument with Cu Kα radiation. UV−vis diffuse reflectance spectra of the samples were obtained on an UV−vis spectrophotometer (Hitachi U-3010) using $BaSO_4$ as the reference. The photodegradation of the MO pollutant was monitored by measuring the real-time UV−vis absorption of MO at 463 nm using a JASCO UV-550 spectrometer. X-ray photoelectron spectroscopy (XPS) was performed on an ESCALab220i-XL electron spectrometer from VG Scientific using 300 W Al Kα radiation. The binding energies were referenced to the C1s line at 284.8 eV from adventitious carbon. The Raman spectra were recorded on a Renishaw inVia plus Raman microscope using a 514.5 nm argon ion laser. All of the measurements were carried out at room temperature.

RESULTS AND DISCUSSION

It has been widely verified that the temperature of a synthesis system could play an important role in determining the shape of the produced nanostructures. A relatively higher temperature favors the formation anisotropically shaped nanospecies, while a lower temperature prefers the production of isotropically shaped counterparts.[37,38] To control the shape of the Ag/AgCl nanospecies, and to visualize the role of GO, we first carried out our nanofabrications at different temperatures in the absence of GO. As shown in Figure 1, when the synthesis was

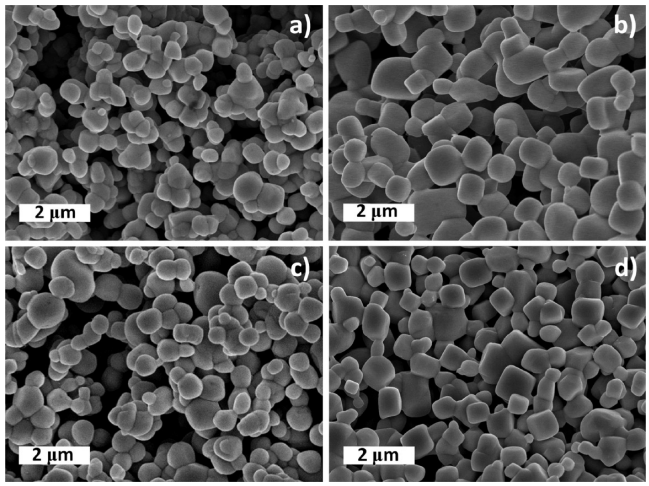

Figure 1. Typical SEM images of the near-spherical (a and c) and cube-like (b and d) Ag/AgCl nanoarchitectures of ca. 500 nm formulated without GO nanosheets. The $AgNO_3$ (a and b) and $Ag(NH_3)_2NO_3$ (c and d) were employed as Ag sources, respectively. The syntheses were carried out at 0 °C (a and c) and 30 °C (b and d), respectively.

performed at 0 °C, near-spherical nanostructures of ca. 500 nm were produced simply by adding a NaCl solution dropwise into a $AgNO_3$ or $Ag(NH_3)_2NO_3$ solution. In contrast, when the similar reactions were performed at 30 °C, cube-like nanospecies of ca. 500 nm were produced. As verified by the aforementioned experimental facts in terms of XRD, XPS, and UV−visible diffuse reflectance spectra, thus-obtained products are plasmonic Ag/AgCl nanospecies, wherein the generation of metallic Ag species is due to the ambient light.[15,20] These results suggest that the shape of Ag/AgCl could be selected by the employed temperature. Meanwhile, it suggests that $AgNO_3$ and $Ag(NH_3)_2NO_3$, which work as silver sources, display reaction behaviors similar to that of NaCl when no GO nanosheets are involved during the synthesis.

We have also carried out parallel fabrications in the presence of GO. In these cases, GO was introduced into the systems prior to the addition of NaCl. As shown in Figure 2a and b, for

dx.doi.org/10.1021/la401473t | Langmuir 2013, 29, 9259−9268

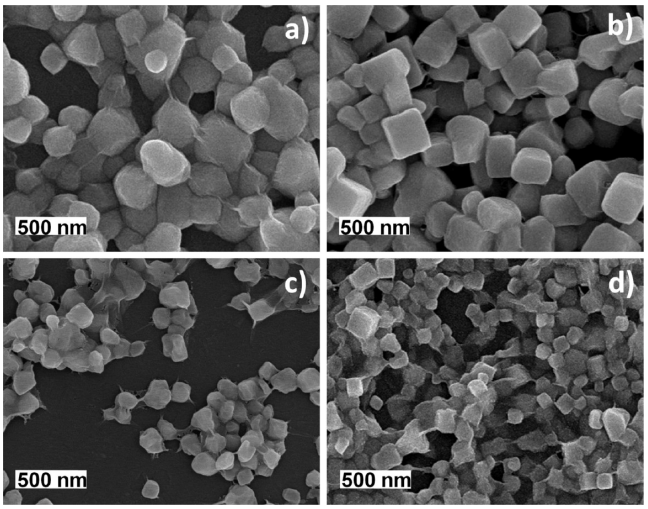

Figure 2. Typical SEM images of the near-spherical (a and c) and cube-like (b and d) Ag/AgCl/GO nanoarchitectures formulated in the presence of the GO. The $AgNO_3$ (a and b) and $Ag(NH_3)_2NO_3$ (c and d) were employed as Ag sources, respectively. The syntheses were carried out at 0 °C (a and c) and 30 °C (b and d), respectively. The size of the nanostructures produced in the $AgNO_3$ (a and b) and $Ag(NH_3)_2NO_3$ (c and d) systems is ca. 200 and 100 nm, respectively.

the $AgNO_3$ system, near-spherical and cube-like nanospecies of ca. 200 nm are produced when a synthetic temperature of 0 and 30 °C is employed, respectively. It is interesting to see that as compared to the corresponding bare Ag/AgCl of the $AgNO_3$ system manufactured without GO, the size of thus-formulated GO-hybridized nanostructures Ag/AgCl/GO is about 2.5 times decreased from ca. 500 to 200 nm. As indicated in Figure 2c and d, in the case of the $Ag(NH_3)_2NO_3$ system, near-spherical and cube-like Ag/AgCl/GO with a size of ca. 100 nm are produced at 0 and 30 °C, respecitively. As compared to the corresponding bare Ag/AgCl nanostructures produced in the $Ag(NH_3)_2NO_3$ system, the size of thus-formulated Ag/AgCl/GO is about 5 times decreased from ca. 500 to 100 nm. Meanwhile, the size of these Ag/AgCl/GO is about 2 times decreased from ca. 200 to 100 nm as compared to their counterparts fabricated in the $AgNO_3$ system.

These interesting facts suggest that the size of the Ag/AgCl of different shape could be reduced when GO is introduced into the synthesis system. As is well-known, GO nanosheets are geometrically two-dimensional graphene segments, on which various oxygen-containing groups are attached.[10] This feature endows GO with interesting physicochemical properties as a water-soluble polymer,[34−36] which are always employed as capping agent or stabilizer in the synthesis of size-controlled nanostructures.[15,19,23] Considering these features of GO, we suggest that in the presence of GO, the produced Ag/AgCl could be capped by GO soon after the chemical reaction of Ag^+ and Cl^-, stunting the further growth of the nanostructures and thus leading to a smaller size. The capping function of GO could be evidently seen from the SEM images of Ag/AgCl/GO, wherein the Ag/AgCl nanoparticles are wrapped by GO, as shown in Figure 2.

The Fourier transform infrared spectra (FT-IR) of our nanostructures were investigated. As shown in Figure S2, our original powdery GO displays two vibrations centered at ca. 1736, 1436 cm^{-1}. The peak at ca. 1736 cm^{-1} is attributed to the C═O stretching vibrations of carboxyl groups,[30,39−41] while that at ca. 1436 cm^{-1} is ascribed to C−O stretching and O−H bending modes of carboxylic acid groups.[42,43] The broad peak centered at ca. 1640−1610 cm^{-1} is ascribed to the vibrations of the adsorbed water and the skeletal vibrations of the unoxidized graphitic domains.[15,40,44] For Ag/AgCl/GO, the GO peaks at ca. 1736 (C═O stretching vibrations of carboxyl groups) and ca. 1436 cm^{-1} (C−O stretching and O−H bending modes of carboxylic acid groups)[30,40−43] shift to lower wavenumbers of ca. 1721 and 1415 cm^{-1}, respectively. As is known, the carboxylic acid group is generally monitored for shifts to verify the bonding or capping of nanoparticles.[15,20,45−47] The wavenumber shift of the carboxylic acid-related bands is due to the transfer of electron density to form a new metal−O bond in the presence of the metal nanoparticle.[15,20,45] Commonly, carboxylic acid bands would have less electron density upon the formation of the new bond. This would lead to a frequency shift to lower wavenumbers. Consequently, the blue shifts observed from the C═O, C−O, and O−H groups suggest the capping or bonding of Ag/AgCl by the carboxylic acid groups of GO, resulting in the formation of GO-hybridized nanostructures, Ag/AgCl/GO.[15,20,45]

As shown in Figure S2, a shoulder band around ca. 1360 cm^{-1} attributed to the symmetric stretching vibrations of carboxylate anion $\nu(COO^-)$[48,49] could also be discerned from the FT-IR spectra of all of the Ag/AgCl/GO nanospecies. In the case of the original powdery GO, this band is almost undiscernible. This indicates that, in addition to the carboxylic acid groups, the Ag/AgCl of Ag/AgCl/GO are also grasped by the carboxylate group of GO. Meanwhile, as compared to that of the Ag/AgCl/GO formulated in $AgNO_3$ system, this shoulder band manifests itself relatively clearer in the case of

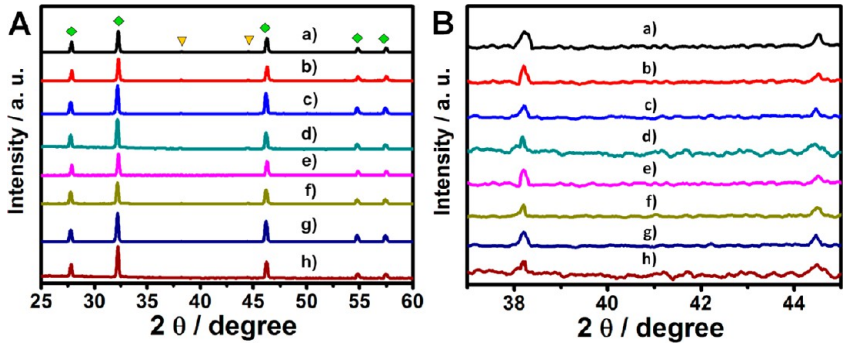

Figure 3. XRD (A) and magnified XRD (B) patterns of the Ag/AgCl (a−d) and Ag/AgCl/GO (e−h) fabricated in $AgNO_3$ (a, c, e, and g) and $Ag(NH_3)_2NO_3$ (b, d, f, and h) systems at 0 °C (a, b, e, and f) and 30 °C (c, d, g, and h).

dx.doi.org/10.1021/la401473t | Langmuir 2013, 29, 9259−9268

the samples fabricated in $Ag(NH_3)_2NO_3$ system. This observation likely suggests that the Ag/AgCl nanospecies are capped by GO with more carboxylate sites in the latter case. The pH value of the $AgNO_3$ synthesis system was ca. 5−6.5, while that of the $Ag(NH_3)_2NO_3$ system was ca. 9.5−10.5. As is known, basic circumstance could promote the ionization of carboxyl groups, leading to the formation of carboxylate anions. Accordingly, the above-mentioned results might be reasonable, because the NH_3 of $Ag(NH_3)_2NO_3$ could promote the ionization of the carboxylic acid groups of GO, leading to the formation of carboxylate anions, which could act as additional capping sites for the hybridization of Ag/AgCl nanoparticles via the electrostatic interactions between the carboxylate anions and silver cations.

On the basis of these facts, it could be proposed that the even smaller size of Ag/AgCl/GO formulated in the $Ag(NH_3)_2NO_3$ system could be due to the NH_3-facilitated capping effect of GO, because the further growth of Ag/AgCl in this system could be inhibited by GO more fruitfully with the additional assistance of the electrostatic interactions between the carboxylate anions and silver cations. It thus can be seen that the introduction of GO into the precipitation reaction between Cl^- and Ag^+ could reduce the size of the produced Ag/AgCl nanospecies, wherein when $Ag(NH_3)_2NO_3$ is employed as silver source, the particle size could be further reduced. Our results also indicate that the morphology of the Ag/AgCl-based nanostructures could be controlled by the temperature of the reaction system, although there exists almost no difference between $AgNO_3$ and $Ag(NH_3)_2NO_3$ when GO is not involved.

To validate the generation of Ag/AgCl-based nanospecies, the structure of our samples was investigated by XRD. As shown in Figure 3, all of the samples, the bare Ag/AgCl and GO-hybridized Ag/AgCl, display distinct diffraction peaks (2θ) at 27.8° (111), 32.2° (200), 46.2° (220), 54.8° (311), and 57.5° (222), which are indexed to the typical cubic phase of AgCl (JCPDS file: 31-1238).[23] Besides, diffraction peaks at 38.2° (111) and 44.6° (200), which are ascribed to the cubic phase of metallic Ag (JCPDS file: 65-2871),[23] could also be observed (for magnified XRD patterns around 37°−45°, Figure 3B). These facts suggest that the as-formulated samples are all Ag/AgCl-based nanomaterials. Note that no diffraction peaks ascribed to GO could be evidently detected from the XRD patterns of the Ag/AgCl/GO species. This is due to the existence of the intercalated Ag/AgCl nanoparticles in the system, which would destroy the regular stack of GO nanosheets.[20] On the other hand, this might also be due to the relatively low diffraction intensity of GO nanosheets.[50]

The components of our nanostructures are investigated by energy dispersive X-ray spectroscopy (EDX) analysis. As shown in Figure S3, for all of the samples fabricated without GO, Cl and Ag elements could be identified. The semiquantitative analysis indicates that the atomic ratio between Ag and Cl is approximately 1.1:1. These data are higher than the theoretic stoichiometric atomic ratio between Ag and Cl in AgCl, which should be 1:1. This fact is in accordance with the information deduced from XRD, further indicating the existence of metallic Ag in the as-formulated samples. As shown in Figure S3, in the cases of the samples fabricated in the presence of GO, almost similar results are obtained except that besides the Ag and Cl (Ag:Cl = 1.1:1), C and O, which are attributed to GO, could also be detected. Together with the facts observed from SEM and FT-IR, these results further verify the existence of GO in the produced nanospecies when GO is involved during the synthesis procedure.

To further disclose the components of our nanostructures, the samples were investigated by XPS. As shown in Figure S4, when GO is not involved in the synthesis systems, the XPS spectra of the samples formulated both in the $AgNO_3$ and in the $Ag(NH_3)_2NO_3$ systems display a binding energy of Cl $2p_3$ and Cl $2p_1$ at about 197.5 and 199.1 eV, respectively.[23] In addition, two bands at ca. 367.1 and 373.2 eV, ascribed to Ag $3d_{5/2}$ and Ag $3d_{3/2}$ binding energies, respectively, could also be observed.[23] The deconvolution of these two bands gives out two couples of peaks at ca. 367.1, 368.1 eV and 373.2, 374.1 eV, respectively. Those around ca. 367.1 and 373.2 eV could be attributed to the Ag^+ of AgCl, while those at ca. 368.1 and 374.1 eV could be ascribed to the metallic Ag^0 species,[21,23,51,52] wherein the surface mole ratio between Ag^+ and Ag^0 is semiquantitatively estimated to be approximately 10:1. These results further verify the existence of Ag^0 in the as-formulated nanospecies, which are in accordance with the facts obtained from the XRD and EDX investigations.

On the other hand, for the samples fabricated in the presence of GO nanosheets, almost similar XPS results are obtained (Figure S4), wherein the semiquantitatively calculated surface mole ratio between Ag^+ and Ag^0 is also roughly 10:1. Meanwhile, as shown in Figure 4, the C1s XPS spectra of

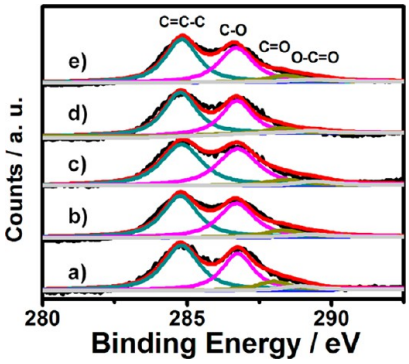

Figure 4. C1s XPS spectra of powders GO (a) and Ag/AgCl/GO (b−e) fabricated in $AgNO_3$ (b and d) and $Ag(NH_3)_2NO_3$ (c and e) systems at 0 °C (b and c) and 30 °C (d and e).

our powdery GO and the Ag/AgCl/GO were also measured. For GO, distinct C1s XPS spectra located at ca. 284.8, 286.6, 288, and 289.1 eV, which are attributed to the C═C−C (sp^2 carbon), C−O, C═O, and O−C═O units of typical GO nanosheets, respectively,[30,53] are observed. A semiquantitative estimation indicates that the atom ratio between oxygen and carbon (O/C) is ca. 0.63. For Ag/AgCl/GO nanostructures, almost similar results are obtained except that the C═O and O−C═O signals shift to higher binding energies to ca. 288.3 and ca. 289.3 eV, respectively, for the Ag/AgCl/GO produced in $AgNO_3$ systems, while to ca. 288.4 and ca. 289.4 eV, for the samples formulated in $Ag(NH_3)_2NO_3$ systems. Together with the results of SEM, EDX, and FT-IR spectra, these facts further indicate the existence of GO in our Ag/AgCl/GO species.

As is known, for the visible-light-energized catalysts, it is necessary that they could display distinct absorptions in the visible region. The UV−visible diffuse reflectance spectra of our nanostructures are illustrated in Figure 5. It can be seen that for all of the samples fabricated with or without GO, broad and strong absorptions in visible region could be detected. In

dx.doi.org/10.1021/la401473t | Langmuir 2013, 29, 9259−9268

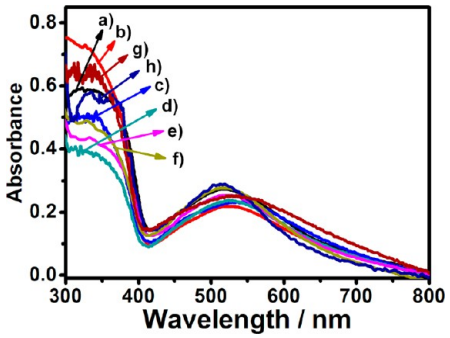

Figure 5. UV−vis diffuse reflectance spectra of the Ag/AgCl (a−d) and Ag/AgCl/GO (e−h) fabricated in $AgNO_3$ (a, c, e, and g) and $Ag(NH_3)_2NO_3$ (b, d, f, and h) systems at 0 °C (a, b, e, and f) and 30 °C (c, d, g, and h).

general, AgCl and GO could only display absorptions in the ultraviolet region but negligible absorption in the visible region.[22,30] Accompanied by the facts obtained from XRD (Figure 3), EDX (Figure S3), and XPS (Figure S4) analyses, these distinct visible-light responsive properties could be due to the existence of metallic Ag^0 in our nanostructures, which could arouse distinct surface plasmon resonance (SPR) absorptions in the visible region.[15−19] This spectral feature might make our Ag/AgCl and Ag/AgCl/GO catalytically active under visible-light irradiation.

On the basis of the above-mentioned experimental facts, it could be seen that by means of introducing GO into the precipitation reaction between Ag^+ and Cl^-, controlling the temperature of the synthesis system, and selecting appropriate silver source, visible-light active plasmonic Ag/AgCl nanospecies with controlled size and shape could be synthetically formulated. This provides us with a significant platform for the investigation of their size- and shape-sensitive photocatalytic activities, wherein high-performance plasmonic photocatalysts might be optimally identified and selected. Along this line of thought, the photocatalytic behavior of our Ag/AgCl-based nanomaterials was investigated in terms of photodegradation of methyl orange (MO) pollutant under visible-light irradiation. To make a clear description for the photocatalytic performances of the series of our Ag/AgCl, the near-spherically shaped samples of 500 nm formulated at 0 °C are designated as Ag/AgCl-500 NS, while those of 500 nm with a cube-like morphology formulated at 30 °C are denoted as Ag/AgCl-500 NC. On the other hand, the near-spherical and cube-like Ag/AgCl/GO nanoarchitectures formulated in the presence of GO are named as Ag/AgCl/GO-200 NS and Ag/AgCl/GO-200 NC, respectively, when $AgNO_3$ is employed as Ag source, while they are designated as Ag/AgCl/GO-100 NS and Ag/AgCl/GO-100 NC, respectively, when $Ag(NH_3)_2NO_3$ is used as Ag source.

Experimentally, prior to light irradiation, a dark adsorption was performed to achieve an equilibrium adsorption state. As shown in Figure 6A, when the bare Ag/AgCl nanostructures, Ag/AgCl-500 NS and Ag/AgCl-500 NC, formulated in the $AgNO_3$ system, are employed as the photocatalysts, ca. 22.3% and 34.3% of MO molecules are decomposed within 16 min, repestively. When the corresponding nanoarchitectures fabricated in $Ag(NH_3)_2NO_3$ system are used as the catalysts, nearly similar results are obtained, as shown in Figure S5. These results are actually reasonable, because as demonstrated in the above sections, the shape, component, size, and optical properties of the samples formulated without GO display a distinct dependence on the temperature of the synthesis systems, while a negligible dependence on Ag sources. On the other hand, it can be seen that when the near-spherical Ag/AgCl/GO-200 NS and Ag/AgCl/GO-100 NS are used as photocatalysts, ca. 65.3% and 86.9% MO molecules are photodegraded under similar experimental conditions, respectively. Significantly, when the cube-like Ag/AgCl/GO-200 NC and Ag/AgCl/GO-100 NC are used as the catalysts, the photocatalytic performance is further enhanced, wherein ca. 94.1% and nearly 100% MO molecules are decomposed within 16 min, respectively. In addition, our results (Figure S6) also showed that the catalytic performances of the bare Ag/AgCl-500 NS and Ag/AgCl-500 NC displayed only slight changes when these nanostructures were mixed with GO. Moreover, when GO was employed as the catalyst, negligible MO molecules could be decomposed (Figure S7). These results indicate that GO could not work as an efficient catalyst.

As plotted in Figure 6B, there is a nice linear correlation between $\ln(C/C_0)$ and the reaction time (t), indicating that the decomposition of MO over our catalysts follows the first-order kinetics. As summarized in Table 1, it can be seen that the rate constants of the catalytic degradation of MO over our Ag/AgCl-500 NS, Ag/AgCl-500 NC, Ag/AgCl/GO-200 NS, Ag/AgCl/GO-100 NS, Ag/AgCl/GO-200 NC, and Ag/AgCl/GO-100 NC are 0.014, 0.023, 0.056, 0.116, 0.17, and 0.284 min^{-1}, respectively, wherein an increase tendency could be evidently observed. Accompanied by the size, shape, and components of these nanostructures, three issues could be derived from these results: (i) as compared to the bare Ag/AgCl nanospecies, the

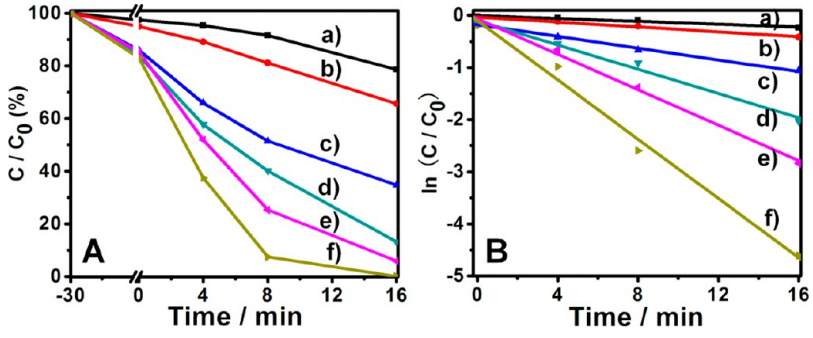

Figure 6. Catalytic activities (A) and kinetic linear simulation curves (B) of the Ag/AgCl-based plasmonic photocatalysts for the degradation of MO under visible light irradiation: Ag/AgCl-500 NS (a), Ag/AgCl-500 NC (b), Ag/AgCl/GO-200 NS (c), Ag/AgCl/GO-100 NS (d), Ag/AgCl/GO-200 NC (e), and Ag/AgCl/GO-100 NC (f).

dx.doi.org/10.1021/la401473t | Langmuir 2013, 29, 9259−9268

Table 1. Summary of the Synthesis of Ag/AgCl-Based Plasmonic Nanoarchitectures with Controlled Size and Shape with or without GO, and the Catalytic Performances of the Formulated Nanostructures for the Photodegradation of MO Pollutant under Visible-Light Irradiations

catalysts	synthesis temp (°C)	shape	Ag source	GO	size (nm)	rate constant of the catalytic reaction (min^{-1})
Ag/AgCl-500 NS[a]	0	near-spherical	$AgNO_3$ or $Ag(NH_3)_2NO_3$	no	500	0.014
Ag/AgCl-500 NC[a]	30	cube-like		no	500	0.023
Ag/AgCl/GO-200 NS	0	near-spherical	$AgNO_3$	yes	200	0.056
Ag/AgCl/GO-100 NS	0	near-spherical	$Ag(NH_3)_2NO_3$	yes	100	0.116
Ag/AgCl/GO-200 NC	30	cube-like	$AgNO_3$	yes	200	0.17
Ag/AgCl/GO-100 NC	30	cube-like	$Ag(NH_3)_2NO_3$	yes	100	0.284

[a]When GO nanosheets are absent from the synthesis medium, almost similar results were obtained using $AgNO_3$ or $Ag(NH_3)_2NO_3$ as the Ag source.

GO-hybridized nanostructures, Ag/AgCl/GO, could display evidently enhanced catalytic activities; (ii) for the nanospecies of the similar shape, those with a smaller size could display higher catalytic performances; and (iii) for the nanoarchitectures of the similar size, the cube-like nanospecies exhibit higher catalytic activities as compared to their near-spherically shaped counterparts. These results suggest the achievement of size- and shape-dependent photocatalytic performances using the series of our Ag/AgCl-based plasmonic nanostructures.

Generally, the adsorptive capacity of a catalyst to the substrate molecules is one of the crucial factors that affects its photocatalytic activity, wherein the higher is the adsorptive capacity, the higher are the catalytic performances.[15,19,50] As shown in Figure 6A and Figure S8, as compared to the bare Ag/AgCl nanospecies, the GO-hybridized Ag/AgCl nanostructures exhibit a higher adsorptive capacity to MO molecules. This could be ascribed to the hybridization of the GO in these systems, which have been proven to favor the adsorption of pollutant molecules via $\pi-\pi$ interactions.[50] This nice adsorptive capacity of Ag/AgCl/GO might contribute partially to their enhanced photocatalytic activity.

On the other hand, it is known that the size of a catalytst could likewise affect its adsorptive ability, wherein a smaller size could facilitate the adsorption and thus promote the catalytic performance.[4−7] At the same time, as compared to those with a bigger size, the catalysts of a smaller size usually have more catalytically active sites, which could also accelerate the catalytic reaction.[4−7,37] These are due to the high surface-to-volume ratio of nanospecies of smaller size.[4−7] As suggested by the SEM images of our samples (Figures 1 and 2), the GO-hybridized Ag/AgCl nanostructures have a smaller size as compared to the bare Ag/AgCl nanospecies. These size effects might also contribute partially to the higher photocatalytic performance of the Ag/AgCl/GO nanostructures.[15] As shown in Figures 2, 6, and S8 and Table 1, this size-sensitive catalytic performance could also manifest itself in the catalytic behaviors of the series of our GO-hybridized catalytsts, wherein the Ag/AgCl/GO-100 NS and Ag/AgCl/GO-100 NC display higher catalytic activities than their counterparts of similar shape, Ag/AgCl/GO-200 NS and Ag/AgCl/GO-200 NC.

As is well-known, an efficient charge separation/transfer is another crucial issue affecting the catalytic performance of a photocatalyst.[31−33] Because of their unique locally conjugated aromatic electronic structure, GO has recently been recognized to be one of the most ideal catalyst promoters in terms of facilitating an electron transfer.[15,28−33] To verify this in our present Ag/AgCl/GO photocatalysts, the electrochemical impedance spectra (EIS) of our GO, the bare Ag/AgCl, and Ag/AgCl/GO were investigated as Nyquist plots, as shown in Figure 7. It can be seen that the size of the arc radius of the Ag/AgCl/GO species is evidently smaller than that of the GO and

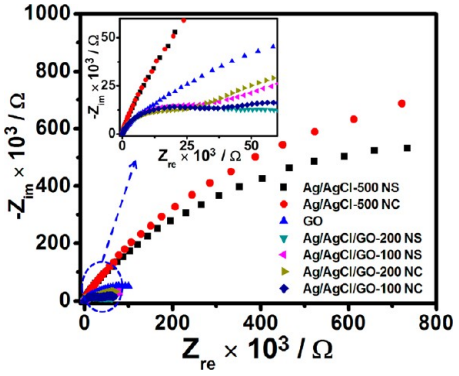

Figure 7. EIS changes of our Ag/AgCl, GO, and Ag/AgCl/GO electrodes. The EIS measurements were performed in the presence a 2.5 mM $K_3[Fe(CN)_6]/K_4[Fe(CN)_6]$ (1:1) mixture as a redox probe in a 0.1 M KCl solution at a potential of 0.1 V.

the bare Ag/AgCl. This suggests a decrease in the solid-state interface layer resistance and the charge transfer resistance on the surface of our Ag/AgCl/GO.[50,53,54] Moreover, the XPS (Figure S4) and Raman (Figure S9) spectral investigations also suggest that the Ag/AgCl and GO species work as electron-donor and electron-acceptor components, respectively, in the Ag/AgCl/GO nanocomposites (for more detailed discussions about these issues, see the Supporting Information). These facts suggest that the electrons originally photogenerated on the plasmonic Ag/AgCl nanospecies could migrate into GO nanosheets through a percolation process[15,20] during the photocatalytic performance. This could promote the charge separation/transfer, and thus suppress the recombination of electron−hole pairs, leading to an enhancement of the photocatalytic performance of Ag/AgCl/GO.[15,20]

As shown in Figures 2, 6, and Table 1, as compared to the near-spherical Ag/AgCl/GO-100 NS, the cube-like Ag/AgCl/GO-200 NC displays higher catalytic performance, although the former has a smaller size. These facts suggest that the enhanced catalytic activities in these catalysts could not be simply interpreted by the above-mentioned size effect, and that the shape of these nanostructures might play an important role. It is known that the shape-selective catalytic activity could generally be understood in terms of the different reaction performances induced by the specific crystal facets selectively exposed by an anisotropically shaped nanostructure.[4−7,55−58] As indicated by the XRD patterns shown in Figure 3, the intensity ratio of ca. 2.4 for the (200) and (111) diffractions of the cube-like

dx.doi.org/10.1021/la401473t | Langmuir 2013, 29, 9259−9268

nanostructures is remarkably higher than the ca. 1.8 of the near-spherical nanospecies. This suggests that our cube-like crystals are relatively dominated by {100} planes.[56−58] As is known, catalytic reactions are sensitive to the surface structure of the catalysts, wherein the crystal plane of the catalyst plays an important role. Generally, the planes with higher surface energy are more reactive.[56,59] The surface energies associated with different crystallographic planes are usually different, and a general sequence may hold, $\gamma(100) > \gamma(111)$.[59] Consequently, the plane of {100} is generally known to be more reactive than that of {111}. On the basis of these facts, the higher catalytic activities of our cube-like Ag/AgCl-based nanostructures as compared to their near-spherical counterparts could be due to their more-reactive {100} planes. Similar proposals have been reported by others.[55−58]

As shown in Figure 6 and summarized in Table 1, it could be seen that the catalytic activity of our cube-like Ag/AgCl/GO-100 NC is substantially higher than that of Ag/AgCl-500 NS, Ag/AgCl-500 NC, Ag/AgCl/GO-200 NS, Ag/AgCl/GO-100 NS, and Ag/AgCl/GO-200 NC by a factor of ca. 20, 12, 5, 2.4, and 1.7, respectively. On the basis of the above-mentioned discussions, it could be proposed that the synergistic effect of size, shape, and GO nanosheets plays a crucial role for its distinctly boosted catalytic performances.

Besides the high catalytic performance, the stability of the catalyst is another important criterion required by excellent catalyst. The durability of our Ag/AgCl/GO-100 NC plasmonic photocatalyst was also evaluated in terms of performing the catalytic performances repeatedly several times. As shown in Figure 8, the catalytic activity displays only a slight decrease

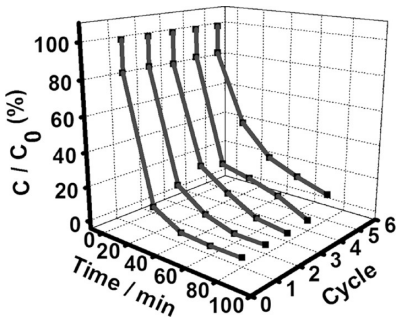

Figure 8. Five consecutive cycling photodegradation curves of MO pollutant over the Ag/AgCl/GO-100 NC photocatalyst under visible light irradiation.

after the catalytic performances are operated five times continuously. As shown in Figure S10, the morphology of this catalyst displays only trivial changes after the bleaching reactions. On the other hand, the durability of our Ag/AgCl-500 NC catalysts produced in the $Ag(NH_3)_2NO_3$ systems was also investigated. As shown in Figure S11, such catalysts in the absence of GO could also display good recycling properties under our experimental conditions. These results suggest that our Ag/AgCl-based nanostructures could be used as highly efficient yet stable plasmonic photocatalysts for the bleaching of organic pollutants, indicating its bright future for potential applications.

CONCLUSION

In summary, in terms of controlling the synthesis temperature, choosing appropriate Ag sources, and hybridizing GO, we have demonstrated that Ag/AgCl-based plasmonic nanostructures with controlled size and shape could be facilely formulated. Our results show that among the series of our nanostructures of different size and shape, the cube-like Ag/AgCl/GO-100 NC displays evidently enhanced catalytic activity. It is suggested that the synergistic effect of size, shape, and GO nanosheets plays an important role. Our investigation indicates that GO works not only as a capping agent during the nanofabrication step, resulting in Ag/AgCl nanostructures of a smaller size, but also as catalyst promoter during the performance of the catalytic reaction, leading to a significantly boosted catalytic activity. Considering the general interest of GO and the broad concerns of the visible-light-energized plasmonic catalysts, our GO-mediated approach might pave a new avenue and open new opportunities for GO-hybridized high-performance catalysts.

ASSOCIATED CONTENT

Supporting Information

AFM image and XRD pattern of our GO; FT-IR spectra, Cl 2p and Ag 3d XPS spectra, EDX and Raman spectra of our nanostructures; real-time absorption spectra of MO during the photodegradation process; catalytic activities of GO, Ag/AgCl-500 NS, Ag/AgCl-500 NC, and those of the mixture of GO and the bare Ag/AgCl nanostructures; SEM image of the Ag/AgCl/GO-100 NC after the photodcatalytic performances; and discussions on the XPS and Raman spectra. This material is available free of charge via the Internet at http://pubs.acs.org.

AUTHOR INFORMATION

Corresponding Author

*E-mail: chenpl@iccas.ac.cn, cpl@zzu.edu.cn (P.C.); liumh@iccas.ac.cn (M.L.).

Notes

The authors declare no competing financial interest.

ACKNOWLEDGMENTS

We acknowledge financial support from the National Natural Science Foundation of China (20873159, 21021003, and 91027042), the National Key Basic Research Project of China (2011CB932301 and 2013CB834504), and CAS (1731300500015). The authors are grateful to Prof. Fen Liu from the Institute of Chemistry, Chinese Academy of Sciences, for her profound discussions concerning the analyses of the XPS spectra. P.C. thanks Zhengzhou University for the "Talent Project of Distinguished Professor".

REFERENCES

(1) Burda, C.; Chen, X. B.; Narayanan, R.; El-Sayed, M. A. Chemistry and Properties of Nanocrystals of Different Shapes. *Chem. Rev.* **2005**, *105*, 1025−1102.

(2) Xia, Y.; Xiong, Y.; Lim, B.; Skrabalak, S. E. Shape-Controlled Synthesis of Metal Nanocrystals: Simple Chemistry Meets Complex Physics? *Angew. Chem., Int. Ed.* **2009**, *48*, 60−103.

(3) Ray, P. C. Size and Shape Dependent Second Order Nonlinear Optical Properties of Nanomaterials and Their Application in Biological and Chemical Sensing. *Chem. Rev.* **2010**, *110*, 5332−5365.

(4) Li, Y.; Liu, Q.; Shen, W. Morphology-Dependent Nanocatalysis: Metal Particles. *Dalton Trans.* **2011**, *40*, 5811−5826.

(5) Chen, J.; Lim, B.; Lee, E. P.; Xia, Y. Shape-Controlled Synthesis of Platinum Nanocrystals for Catalytic and Electrocatalytic Applications. *Nano Today* **2009**, *4*, 81−95.

(6) Wang, D.; Xie, T.; Li, Y. Nanocrystals: Solution-Based Synthesis and Applications as Nanocatalysts. *Nano Res.* **2009**, *2*, 30−46.

(7) Semagina, N.; Kiwi-Minsker, L. Recent Advances in the Liquid-Phase Synthesis of Metal Nanostructures with Controlled Shape and Size for Catalysis. *Catal. Rev.* **2009**, *51*, 147−217.
(8) Linic, S.; Christopher, P.; Ingram, D. B. Plasmonic-Metal Nanostructures for Efficient Conversion of Solar to Chemical Energy. *Nat. Mater.* **2011**, *10*, 911−921.
(9) Wang, P.; Huang, B.; Dai, Y.; Whangbo, M.-H. Plasmonic Photocatalysts: Harvesting Visible Light with Noble Metal Nanoparticles. *Phys. Chem. Chem. Phys.* **2012**, *14*, 9813−9825.
(10) Zhou, X.; Liu, G.; Yu, J.; Fan, W. Surface Plasmon Resonance-Mediated Photocatalysis by Noble Metal-Based Composites under Visible Light. *J. Mater. Chem.* **2012**, *22*, 21337−21354.
(11) Zhu, M.; Chen, P.; Liu, M. Ag/AgX (X = Cl, Br, I): a New Type Plasmonic Photocatalysts. *Prog. Chem.* **2013**, *25*, 209−220.
(12) Chen, X.; Zhu, H.-Y.; Zhao, J.-C.; Zheng, Z.-F.; Gao, X.-P. Visible-Light-Driven Oxidation of Organic Contaminants in Air with Gold Nanoparticle Catalysts on Oxide Supports. *Angew. Chem., Int. Ed.* **2008**, *47*, 5353−5356.
(13) Awazu, K.; Fujimaki, M.; Rockstuhl, C.; Tominaga, J.; Murakami, H.; Ohki, Y.; Yoshida, N.; Watanabe, T. A Plasmonic Photocatalyst Consisting of Silver Nanoparticles Embedded in Titanium Dioxide. *J. Am. Chem. Soc.* **2008**, *130*, 1676−1680.
(14) Liu, Z.; Hou, W.; Pavaskar, P.; Aykol, M.; Cronin, S. B. Plasmon Resonant Enhancement of Photocatalytic Water Splitting under Visible Illumination. *Nano Lett.* **2011**, *11*, 1111−1116.
(15) Zhu, M.; Chen, P.; Liu, M. Graphene Oxide Enwrapped Ag/AgX (X = Br, Cl) Nanocomposite as a Highly Efficient Visible-Light Plasmonic Photocatalyst. *ACS Nano* **2011**, *5*, 4529−4536.
(16) Wang, P.; Huang, B.; Qin, X.; Zhang, X.; Dai, Y.; Wei, J.; Whangbo, M.-H. Ag@AgCl: A Highly Efficient and Stable Photocatalyst Active under Visible Light. *Angew. Chem., Int. Ed.* **2008**, *47*, 7931−7933.
(17) An, C.; Peng, S.; Sun, Y. Facile Synthesis of Sunlight-Driven AgCl:Ag Plasmonic Nanophotocatalyst. *Adv. Mater.* **2010**, *22*, 2570−2574.
(18) Wang, P.; Huang, B.; Zhang, X.; Qin, X.; Jin, H.; Dai, Y.; Wang, Z.; Wei, J.; Zhan, J.; Wang, S.; Wang, J.; Whangbo, M.-H. Highly Efficient Visible-Light Plasmonic Photocatalyst Ag@AgBr. *Chem.-Eur. J.* **2009**, *15*, 1821−1824.
(19) Zhu, M.; Chen, P.; Liu, M. Ag/AgBr/Graphene Oxide Nanocomposite Synthesized via Oil/Water and Water/Oil Microemulsions: A Comparison of Sunlight Energized Plasmonic Photocatalytic Activity. *Langmuir* **2012**, *28*, 3385−3390.
(20) Zhu, M.; Chen, P.; Liu, M. Highly Efficient Visible-Light-Driven Plasmonic Photocatalysts Based on Graphene Oxide-Hybridized One-Dimensional Ag/AgCl Heteroarchitectures. *J. Mater. Chem.* **2012**, *22*, 21487−21494.
(21) Jiang, J.; Zhang, L. Rapid Microwave-Assisted Nonaqueous Synthesis and Growth Mechanism of AgCl/Ag, and Its Daylight-Driven Plasmonic Photocatalysis. *Chem.-Eur. J.* **2011**, *17*, 3710−3717.
(22) Zhu, M.; Chen, P.; Ma, W.; Lei, B.; Liu, M. Template-Free Synthesis of Cube-like Ag/AgCl Nanostructures via a Direct-Precipitation Protocol: Highly Efficient Sunlight-Driven Plasmonic Photocatalysts. *ACS Appl. Mater. Interfaces* **2012**, *4*, 6386−6392.
(23) Zhu, M.; Chen, P.; Liu, M. Sunlight-Driven Plasmonic Photocatalysts Based on Ag/AgCl Nanostructures Synthesized via an Oil-in-Water Medium: Enhanced Catalytic Performance by Morphology Selection. *J. Mater. Chem.* **2011**, *21*, 16413−16419.
(24) Han, L.; Wang, P.; Zhu, C.; Zhai, Y.; Dong, S. Facile Solvothermal Synthesis of Cube-Like Ag@AgCl: a Highly Efficient Visible Light Photocatalyst. *Nanoscale* **2011**, *3*, 2931−2935.
(25) Chen, D.; Yoo, S. H.; Huang, Q.; Ali, G.; Cho, S. O. Sonochemical Synthesis of Ag/AgCl Nanocubes and Their Efficient Visible-Light-Driven Photocatalytic Performance. *Chem.-Eur. J.* **2012**, *18*, 5192−5200.
(26) An, C.; Wang, R.; Wang, S.; Zhang, X. Converting AgCl Nanocubes to Sunlight-Driven Plasmonic AgCl: Ag Nanophotocatalyst with High Activity and Durability. *J. Mater. Chem.* **2011**, *21*, 11532−11536.
(27) Tang, Y.; Jiang, Z.; Xing, G.; Li, A.; Kanhere, P. D.; Zhang, Y.; Sum, T. C.; Li, S.; Chen, X.; Dong, Z.; Chen, Z. Efficient Ag@AgCl Cubic Cage Photocatalysts Profit from Ultrafast Plasmon-Induced Electron Transfer Processes. *Adv. Funct. Mater.* **2013**, *23*, 2932−2940.
(28) Dreyer, D. R.; Park, S.; Bielawski, C. W.; Ruoff, R. S. The Chemistry of Graphene Oxide. *Chem. Soc. Rev.* **2010**, *39*, 228−240.
(29) Zhou, D.; Cui, Y.; Han, B. Graphene-Based Hybrid Materials and Their Applications in Energy Storage and Conversion. *Chin. Sci. Bull.* **2012**, *57*, 2983−2994.
(30) Ou, X.; Jiang, L.; Chen, P.; Zhu, M.; Hu, W.; Liu, M.; Zhu, J.; Ju, H. Highly Stable Graphene-Based Multilayer Films Immobilized via Covalent Bonds and Their Applications in Organic Field-Effect Transistors. *Adv. Funct. Mater.* **2013**, *23*, 2422−2435.
(31) Xiang, Q.; Yu, J.; Jaroniec, M. Graphene-Based Semiconductor Photocatalysts. *Chem. Soc. Rev.* **2012**, *41*, 782−796.
(32) An, X.; Yu, J. C. Graphene-Based Photocatalytic Composites. *RSC Adv.* **2011**, *1*, 1426−1434.
(33) Zhang, N.; Zhang, Y.; Xu, Y.-J. Recent Progress on Graphene-Based Photocatalysts: Current Status and Future Perspectives. *Nanoscale* **2012**, *4*, 5792−5813.
(34) Kim, J.; Cote, L. J.; Huang, J. Two Dimensional Soft Material: New Faces of Graphene Oxide. *Acc. Chem. Res.* **2012**, *45*, 1356−1364.
(35) Bai, H.; Li, C.; Shi, G. Functional Composite Materials Based on Chemically Converted Graphene. *Adv. Mater.* **2011**, *23*, 1089−1115.
(36) Zhu, M.; Chen, P.; Liu, M. Visible-Light-Driven Ag/Ag_3PO_4-Based Plasmonic Photocatalysts: Enhanced Photocatalytic Performance by Hybridization with Graphene Oxide. *Chin. Sci. Bull.* **2013**, *58*, 84−91.
(37) Tsung, C.-K.; Kuhn, J. N.; Huang, W.; Aliaga, C.; Hung, L.-I.; Somorjai, G. A.; Yang, P. Sub-10 nm Platinum Nanocrystals with Size and Shape Control: Catalytic Study for Ethylene and Pyrrole Hydrogenation. *J. Am. Chem. Soc.* **2009**, *131*, 5816−5822.
(38) Lim, W. P.; Zhang, Z.; Low, H. Y.; Chin, W. S. Preparation of Ag_2S Nanocrystals of Predictable Shape and Size. *Angew. Chem., Int. Ed.* **2004**, *43*, 5685−5689.
(39) Zhang, D.-D.; Zu, S.-Z.; Han, B.-H. Inorganic−Organic Hybrid Porous Materials Based on Graphite Oxide Sheets. *Carbon* **2009**, *47*, 2993−3000.
(40) Stankovich, S.; Piner, R. D.; Nguyen, S. T.; Ruoff, R. S. Synthesis and Exfoliation of Isocyanate-Treated Graphene Oxide Nanoplatelets. *Carbon* **2006**, *44*, 3342−3347.
(41) Titelman, G. I.; Gelman, V.; Bron, S.; Khalfin, R. L.; Cohen, Y.; Bianco-Peled, H. Characteristics and Microstructure of Aqueous Colloidal Dispersions of Graphite Oxide. *Carbon* **2005**, *43*, 641−649.
(42) Viinikanoja, A.; Wang, Z.; Kauppila, J.; Kvarnstrom, C. Electrochemical Reduction of Graphene Oxide and Its in situ Spectroelectrochemical Characterization. *Phys. Chem. Chem. Phys.* **2012**, *14*, 14003−14009.
(43) Xu, G.; Chen, X.; Hu, J.; Yang, P.; Yang, D.; Wei, L. Immobilization of Trypsin on Graphene Oxide for Microwave-Assisted on-Plate Proteolysis Combined with MALDI-MS Analysis. *Analyst* **2012**, *137*, 2757−2761.
(44) Yan, X.; Chen, J.; Yang, J.; Xue, Q.; Miele, P. Fabrication of Free-Standing, Electrochemically Active, and Biocompatible Graphene Oxide−Polyaniline and Graphene−Polyaniline Hybrid Papers. *ACS Appl. Mater. Interfaces* **2010**, *2*, 2521−2529.
(45) Petroski, J.; El-Sayed, M. A. FTIR Study of the Adsorption of the Capping Material to Different Platinum Nanoparticle Shapes. *J. Phys. Chem. A* **2003**, *107*, 8371−8375.
(46) Zhu, M.; Li, Z.; Du, Y.; Mou, Z.; Yang, P. Stable and Efficient Homogeneous Photocatalytic H2 Evolution Based on Water Soluble Pyrenetetrasulfonic Acid Functionalized Platinum Nanocomposites. *ChemCatChem* **2012**, *4*, 112−117.
(47) Zhu, M.; Li, Z.; Xiao, B.; Lu, Y.; Du, Y.; Yang, P.; Wang, X. Surfactant Assistance in Improvement of Photocatalytic Hydrogen Production with the Porphyrin Noncovalently Functionalized Graphene Nanocomposite. *ACS Appl. Mater. Interfaces* **2013**, *5*, 1732−1740.

(48) Bronstein, L. M.; Huang, X.; Retrum, J.; Schmucker, A.; Pink, M.; Stein, B. D.; Dragnea, B. Influence of Iron Oleate Complex Structure on Iron Oxide Nanoparticle Formation. *Chem. Mater.* **2007**, *19*, 3624−3632.
(49) Lu, Y.; Miller, J. D. Carboxyl Stretching Vibrations of Spontaneously Adsorbed and LB-Transferred Calcium Carboxylates as Determined by FTIR Internal Reflection Spectroscopy. *J. Colloid Interface Sci.* **2002**, *256*, 41−52.
(50) Zhang, H.; Lv, X.; Li, Y.; Wang, Y.; Li, J. P25−Graphene Composite as a High Performance Photocatalyst. *ACS Nano* **2009**, *4*, 380−386.
(51) Wagner, C. D., Riggs, W. M., Davis, L. E., Moulder, J. F., Muilenberg, G. E., Eds. *Handbook of X-Ray Photoelectron Spectroscopy: A Reference Book of Standard Data for Use in X-ray Photoelectron Spectroscopy*; Perkin-Elmer: Eden Prairie, MN, 1979.
(52) Gaarenstroom, S. W.; Winograd, N. Initial and Final State Effects in the ESCA Spectra of Cadmium and Silver Oxides. *J. Chem. Phys.* **1977**, *67*, 3500−3506.
(53) Yao, Z.; Zhu, M.; Jiang, F.; Du, Y.; Wang, C.; Yang, P. Highly Efficient Electrocatalytic Performance Based on Pt Nanoflowers Modified Reduced Graphene Oxide/Carbon Cloth Electrode. *J. Mater. Chem.* **2012**, *22*, 13707−13713.
(54) Ling, Y. Y.; Huang, Q. A.; Zhu, M. S.; Feng, D. X.; Li, X. Z.; Wei, Y. A Facile One-Step Electrochemical Fabrication of Reduced Graphene Oxide−Multiwall Carbon Nanotubes−Phospotungstic Acid Composite for Dopamine Sensing. *J. Electroanal. Chem.* **2013**, *693*, 9−15.
(55) Jin, M.; Zhang, H.; Xie, Z.; Xia, Y. Palladium Nanocrystals Enclosed by {100} and {111} Facets in Controlled Proportions and Their Catalytic Activities for Formic Acid Oxidation. *Energy Environ. Sci.* **2012**, *5*, 6352−6357.
(56) Xu, R.; Wang, D.; Zhang, J.; Li, Y. Shape-Dependent Catalytic Activity of Silver Nanoparticles for the Oxidation of Styrene. *Chem. Asian J.* **2006**, *1*, 888−893.
(57) Bi, Y.; Hu, H.; Ouyang, S.; Lu, G.; Cao, J.; Ye, J. Photocatalytic and Photoelectric Properties of Cubic Ag_3PO_4 Sub-Microcrystals with Sharp Corners and Edges. *Chem. Commun.* **2012**, *48*, 3748−3750.
(58) Wang, H.; Li, Y.; Li, C.; He, L.; Guo, L. Facile Synthesis of AgBr Nanocubes for Highly Efficient Visible Light Photocatalysts. *CrystEngComm* **2012**, *14*, 7563−7566.
(59) Wang, Z. L. Transmission Electron Microscopy of Shape-Controlled Nanocrystals and Their Assemblies. *J. Phys. Chem. B* **2000**, *104*, 1153−1175.